A&A 539, A50 (2012)
DOI: 10.1051/0004-6361/201118177


Astronomy & Astrophysics

# Measuring differential rotation of the K-giant $\zeta$ Andromedae$^\star$ *(Research Note)*

Zs. Kővári[1], H. Korhonen[2,3], L. Kriskovics[1], K. Vida[1], J.-F. Donati[4], H. Le Coroller[5], J. D. Monnier[6], E. Pedretti[7], and P. Petit[4,8]

[1] Konkoly Observatory of the Hungarian Academy of Sciences, Konkoly Thege út 15-17, 1121 Budapest XII, Hungary
e-mail: kovari@konkoly.hu
[2] Niels Bohr Institute, University of Copenhagen, Juliane Maries Vej 30, 2100 København Ø, Denmark
[3] Finnish Centre for Astronomy with ESO (FINCA), University of Turku, Väisäläntie 20, 21500 Piikkiö, Finland
[4] IRAP-UMR 5277, CNRS & Univ. de Toulouse, 14 Av. E. Belin, 31400 Toulouse, France
[5] Observatoire de Haute-Provence, OHP/CNRS, 04870 Saint-Michel l'Observatoire, France
[6] University of Michigan, 941 Dennison Building, 500 Church Street, Ann Arbor, MI 48109-1090, USA
[7] ESO, Karl-Schwarzschild Strasse 2, 85748 Garching bei München, Germany
[8] LATT-UMR 5572, CNRS & Univ. P. Sabatier, 14 Av. E. Belin, 31400 Toulouse, France

Received 29 September 2011 / Accepted 20 January 2012

**ABSTRACT**

*Aims.* We investigate the temporal spot evolution of the K-giant component in the RS CVn-type binary system $\zeta$ Andromedae to establish its surface differential rotation.
*Methods.* Doppler imaging was used to study three slightly overlapping spectroscopic datasets, which were obtained independently at three different observing sites. Each dataset covers one full stellar rotation with good phase coverage, which results in a continuous coverage of almost three stellar rotations ($P_{\rm rot}$ = 17.8 d). Therefore, these data are well-suited for reconstructing surface temperature maps and studying temporal evolution in spot configurations. Surface differential rotation was measured by the means of cross-correlation of all possible image pairs.
*Results.* The individual Doppler reconstructions agree well in the revealed spot pattern, recovering numerous low-latitude spots with temperature contrasts of up to ≈1000 K with respect to the unspotted photosphere, and also an asymmetric polar cap that is diminishing with time. Our detailed cross-correlation study consistently indicates solar-type differential rotation with an average surface shear $\alpha \approx 0.055$, in agreement with former results.

**Key words.** stars: activity – stars: imaging – stars: late-type – starspots – stars: individual: $\zeta$ Andromedae

## 1. Introduction

Stellar activity involves a range of magnetic activity phenomena, which are generated and modulated by the dynamo mechanism. The differential rotation is of utmost importance in understanding the magnetic activity, since it is a key element of the stellar dynamo, which has a controlling influence over the strength of the generated magnetic fields, and hence that of the activity itself. The differential rotation on stars with convective envelopes constrains the large-scale topology of the magnetic field, which in turn yields important information on the working of the dynamo beneath the surface. Nevertheless, on stars the detection of the surface differential rotation still remains a challenging observational task, since stellar surfaces, except in rare cases (e.g., Gilliland & Dupree 1996; Monnier et al. 2007), cannot yet be resolved directly. Therefore indirect surface reconstruction techniques such as Doppler imaging (see, e.g., Vogt et al. 1987; Piskunov et al. 1990) is needed. Moreover, because starspots are commonly regarded as tracers of photospheric plasma motions, the pattern of surface differential rotation can be evolved by investigating the short-term spot redistribution through reconstructed time-series surface images (e.g., Donati & Collier Cameron 1997; Weber & Strassmeier 2001; Kővári et al. 2004, 2007a; Barnes et al. 2005; Hussain et al. 2006; Weber 2007, etc.).

We studied the differential rotation of the K-giant component in the long-period RS CVn binary $\zeta$ Andromedae ($\zeta$ And). $\zeta$ And (HD 4502) is a single-lined spectroscopic binary with a bright ($V$ = +4.1 from SIMBAD) K-giant ellipsoidal variable component (Campbell et al. 1911), and an unseen companion of likely late-G or early-K dwarf (Kővári et al. 2007b, hereafter Paper I, see also the references therein). Although its photometric variability is ruled by the ellipticity effect, light-curve modulation with a rotational cycle of 17.8 d is also present, suggesting spot activity (cf. Strassmeier et al. 1989). This feature agrees with the strong Ca II $H\&K$ emission reported first by Joy & Wilson (1949). The star is known also from its H$\alpha$, $UV$, and X-ray activity (cf. Eaton 1995; Reimers 1980; and Schrijver et al. 1984, respectively).

The first extended study of the target using photometric modelling and Doppler imaging was presented in Paper I. Doppler maps revealed spots dominating at lower to medium latitudes with a typical temperature contrast of ≈750 K, as well as a weak and variable polar cap. Considering the distorted geometry, the fundamental system and stellar parameters were specified and an investigation for differential rotation was

$^\star$ Based on observations collected using the Bernard Lyot Telescope at Pic du Midi Observatory; the 1.93-m telescope at Haute-Provence Observatory, France; and the 8.2-m Kueyen telescope (VLT/UT2) of the European Southern Observatory, Chile (Prg. 081.D-0216(A)).

presented. Recently, Korhonen et al. (2010, hereafter Paper II) measured the angular diameter of the star with the Very Large Telescope Interferometer (VLTI/AMBER) and specified its absolute dimensions. A new Doppler image was also reconstructed from the high-quality spectra obtained simultaneously from the VLT/UVES instrument. The resulting image, similarly to the ones in Paper I, recovered mainly cool spots at lower latitudes, amongst which the most dominant features concentrating at quadrature positions, and also some polar features, but with significantly weaker contrast.

A unique opportunity presented itself during August and September 2008, when the star was measured almost consecutively from Pic du Midi Observatory (France), from Haute-Provence Observatory (France), and from the European Southern Observatory (ESO, Chile, see Paper II), providing three independent (slightly overlapping) spectroscopic datasets, each of them suitable to reconstruct one single Doppler image using four favourable mapping lines. In Sect. 2 a brief review of the three datasets is given, then, in Sect. 3, the results from Doppler imaging are presented. Afterwards, in Sect. 4 the Doppler maps are compared with each other by using our sophisticated cross-correlation technique to search for the surface differential rotation pattern. Finally, the results are summarized and discussed in Sect. 5.

## 2. Spectroscopic observations

The spectroscopic data were collected at three different observing sites independently, between 13 August and 1 October, 2008. Each dataset covers roughly one stellar rotation (16−18 days) and the consecutive sets overlap one another by 1−2 days. In all three cases, the covered wavelengths include the 6400 Å region commonly used for Doppler imaging. This contains, amongst others, the mapping lines Fe I-6411, Fe I-6421, Fe I-6430 and Ca I-6439. The summary of the observations is given in Table 1.

All spectra are phased using the same ephemeris as in Paper I, fitting the zero phase to the conjunction with the secondary in front:

$$\mathrm{HJD} = 2\,449\,997.223 \pm 0.017 + 17.769426 \pm 0.000040 \times E. \quad (1)$$

NARVAL spectra. The first dataset in the time-series with a total of 48 spectra was obtained during ten nights between 13–31 August at Pic du Midi Observatory (France) using the 2-m Bernard Lyot Telescope, equipped with the NARVAL spectrograph (Aurière 2003). The spectrograph covers the wavelength range between 3700 Å and 10 000 Å with a resolving power ($\lambda/\Delta\lambda$) of 60 000. Each observation consists of four 30 s long exposures obtained immediately after each other. These exposures were combined into one observation to increase the signal-to-noise ratio (S/N). This way ten individual observations (one per night) from different rotational phases were obtained. The information in Table 1 is for the combined observations. The reference HJD of the Doppler map calculated from the NARVAL spectra in Sect. 3 (i.e., the mean HJD) is 2454702.088.

SOPHIE spectra. The second set consisting of 10 spectra were collected between 30 August and 15 September, 2008 with the SOPHIE échelle spectrograph (Perruchot et al. 2008) at the 1.93-m telescope of Haute-Provence Observatory (France). The spectrograph has a wavelength range of 3872−6943 Å. The observations were carried out in the high-efficiency mode (HE) using 100 $\mu$m fibre, which gives $\lambda/\Delta\lambda$ of 40 000. The exposure time was usually 120 s, but in two cases longer times were used: on September 6 the exposure time was 950 s and on September 11 166 s. The mean HJD of the SOPHIE observations is 2454715.177.

**Table 1.** Observational records of our spectroscopic data.

| HJD 2 454 000+ | Phase[a] | S/N | Date (2008) | Instrument | $n^b$ | $t_{\rm exp}{}^c$ [s] |
|---|---|---|---|---|---|---|
| 691.5464 | 0.178 | 446 | 13 Aug | NARVAL | 4 | 30 |
| 696.5723 | 0.461 | 258 | 18 Aug | NARVAL | 4 | 30 |
| 699.6046 | 0.632 | 242 | 21 Aug | NARVAL | 4 | 30 |
| 701.5989 | 0.744 | 679 | 23 Aug | NARVAL | 4 | 30 |
| 702.5645 | 0.798 | 384 | 24 Aug | NARVAL | 4 | 30 |
| 703.5135 | 0.852 | 270 | 25 Aug | NARVAL | 4 | 30 |
| 704.5673 | 0.911 | 296 | 26 Aug | NARVAL | 4 | 30 |
| 705.5435 | 0.966 | 329 | 27 Aug | NARVAL | 4 | 30 |
| 708.6240 | 0.139 | 421 | 30 Aug | SOPHIE | 1 | 120 |
| 708.6278 | 0.140 | 371 | 30 Aug | NARVAL | 4 | 30 |
| 709.5420 | 0.191 | 445 | 31 Aug | SOPHIE | 1 | 120 |
| 709.6025 | 0.194 | 291 | 31 Aug | NARVAL | 4 | 30 |
| 710.5015 | 0.245 | 335 | 01 Sep | SOPHIE | 1 | 120 |
| 711.6389 | 0.309 | 441 | 02 Sep | SOPHIE | 1 | 120 |
| 714.6815 | 0.480 | 261 | 05 Sep | SOPHIE | 1 | 120 |
| 715.6242 | 0.533 | 198 | 06 Sep | SOPHIE | 1 | 950 |
| 717.4957 | 0.639 | 269 | 08 Sep | SOPHIE | 1 | 120 |
| 718.5432 | 0.698 | 441 | 09 Sep | SOPHIE | 1 | 120 |
| 720.5707 | 0.812 | 237 | 11 Sep | SOPHIE | 1 | 166 |
| 722.8167 | 0.940 | 866 | 13 Sep | UVES | 3 | 8 |
| 724.5445 | 0.035 | 258 | 15 Sep | SOPHIE | 1 | 120 |
| 724.7046 | 0.046 | 650 | 15 Sep | UVES | 3 | 8 |
| 726.7101 | 0.159 | 586 | 17 Sep | UVES | 3 | 8 |
| 727.6870 | 0.214 | 628 | 18 Sep | UVES | 3 | 8 |
| 728.7387 | 0.273 | 762 | 19 Sep | UVES | 3 | 8 |
| 730.7203 | 0.384 | 693 | 21 Sep | UVES | 3 | 8 |
| 732.7287 | 0.497 | 914 | 23 Sep | UVES | 3 | 8 |
| 734.6517 | 0.606 | 785 | 25 Sep | UVES | 3 | 8 |
| 736.6936 | 0.721 | 612 | 27 Sep | UVES | 3 | 8 |
| 740.7533 | 0.949 | 802 | 01 Oct | UVES | 3 | 8 |

**Notes.** [a] Phases computed using Eq. (1). [b] Number of exposures combined into a final spectrum. [c] Lengths of the single exposures.

UVES spectra. The third set of observations were carried out at the ESO with the UVES (UV-Visual Echelle Spectrograph, Dekker et al. 2000) spectrograph mounted on the 8.2-m Kueyen VLT unit telescope. The data were collected during ten nights between 13 September and 1 October, 2008. In the observations the red arm standard wavelength setting of 600 nm was used with image slicer #3. This configuration gives a resolving power ($\lambda/\Delta\lambda$) of 110 000 and a wavelength coverage of 5000−7000 Å. For every observation the three 8 s exposures obtained immediately after each other were combined into a single, very high S/N spectrum. For more details see Paper II. Computing the average HJD we obtain 2454730.621.

## 3. Doppler imaging with TempMap$_\epsilon$

The three datasets cover roughly one stellar rotation, and therefore allow one to reconstruct one Doppler image for each set. For the surface image reconstruction we started from the Doppler imaging code TempMap (Rice et al. 1989) which, afterwards, was extended by us (TempMap$_\epsilon$, Paper I) to take into account the non-spherical shape of stars in close binary systems. In our

approximation, the real Roche-geometry is simplified to a rotation ellipsoid that is elongated towards the other component. We note here that TempMap$_\epsilon$ is the only Doppler imaging code available so far that can use non-spherical surface geometry. We also note that neglecting the ellipticity in the Doppler reconstruction would yield a significant rise in the goodness-of-fit value of the line profile inversion (see Papers I-II). Eventually, the astrophysical input data of $\zeta$ And, including the most feasible distortion parameter, were adopted from Paper I (Table 2 therein).

Doppler imaging was performed for a sample of well-known mapping lines that usually produces the most reliable outcome. In practice, we used only those lines that are jointly covered by all three datasets: Fe I-6411, Fe I-6421, Fe I-6430 and Ca I-6439. The resulting Doppler images are plotted in Fig. 1. Although a higher resolving power would allow for a larger amount of grid points to be used in the map, for comparison reasons we used the same grid size of $5° \times 5°$ in all maps. The individual reconstructions agree well in the revealed spot pattern, i.e., numerous low-latitude spots are recovered with temperature contrasts of up to $\approx$1000 K with respect to the undisturbed photosphere of 4600 K. In addition, an asymmetric cool polar feature is also present at around $\phi \approx 0.75$, however, switching from the NARVAL map to the SOPHIE and UVES maps, i.e., from August to September 2008, the contrast became weaker and the spot concentration shifted backwards in phase. We also refer to Paper II, where a thorough Doppler imaging study was carried out using the UVES observations.

## 4. Cross-correlation study

Surface differential rotation (DR) of a spotted star can be measured by cross-correlation of subsequent Doppler images (Donati & Collier Cameron 1997). Nevertheless, even when reliable Doppler images are available, short-term spot changes (e.g., vivid interaction between neighbouring spots, emerging of a new spot or disintegrating of an old one, etc.) can easily mask the trace of the surface DR in the cross-correlation function (CCF) map. To emphasize the DR pattern, and to diminish differences originating from individual spot motion and evolution, we used our newly developed cross-correlation technique ACCORD ("Average Cross-CORrelation of time-series Doppler images", see e.g., in Kővári et al. 2004, 2007a, Paper I). The basic idea of the method is that the more CCF maps are averaged, the better the result that can be achieved by boosting the cross-correlation features that are jointly present, like the DR pattern itself.

From the Doppler maps shown in Fig. 1 three cross-correlation pairs can be formed: NARVAL/SOPHIE, NARVAL/UVES, and SOPHIE/UVES. Those CCF maps can then be averaged. However, a simple averaging will not boost definitely the DR pattern, because the shape of the correlation pattern depends on the time gap between the paired Doppler images, i.e., the longer the time gap, the longer the elongation of the individual 1D longitudinal cross-correlation functions parallel to the equator (in practice, these are longitude strips in bins of 5°, see, e.g., Kővári et al. 2004). Therefore a linear renormalization must be made before averaging to avoid fuzziness. When the final average CCF map is assembled, the best-correlating pattern can be fitted by an assumed form of the DR law. The result of applying ACCORD to the three Doppler images is plotted in Fig. 2. For the latitude ($\beta$)-dependent rotation law we assumed the usual quadratic form of $\Omega(\beta) = \Omega_{\rm eq}\ (1 - \alpha \sin^2 \beta)$, where $\Omega_{\rm eq}$ is the equatorial angular velocity and $\alpha = (\Omega_{\rm eq} - \Omega_{\rm pole})/\Omega_{\rm eq}$ is the dimensionless

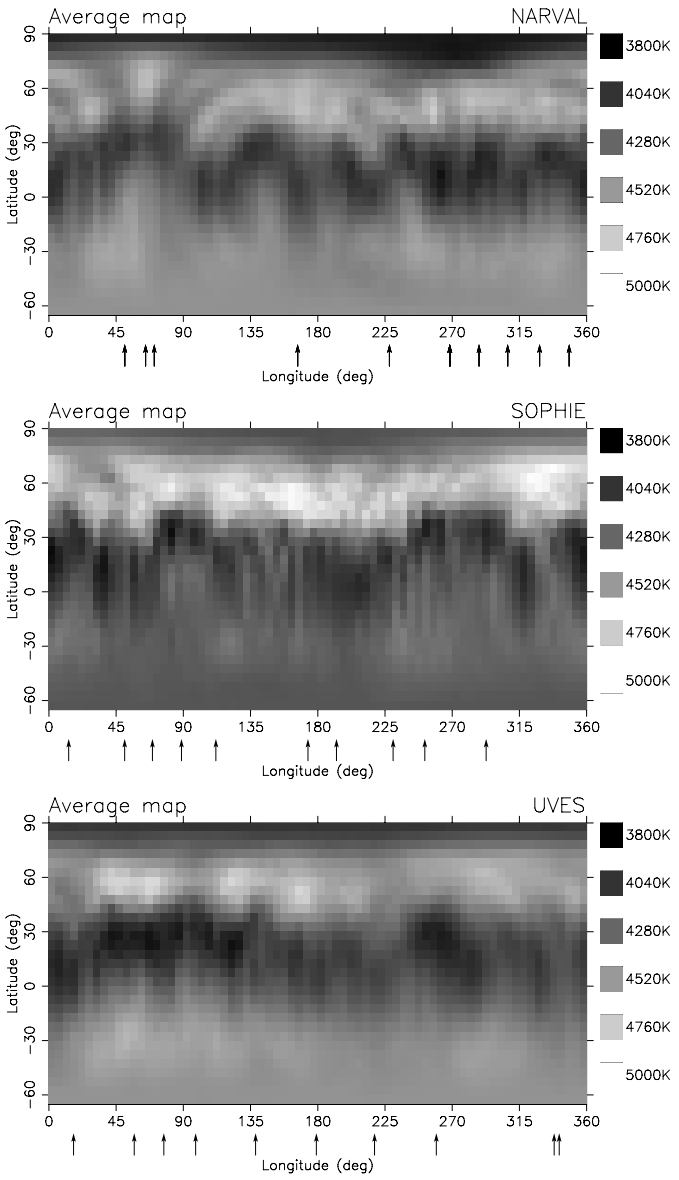


**Fig. 1.** From *top to bottom*: the combined (Fe I-6411+Fe I-6421+ Fe I-6430+Ca I-6439) Doppler maps in time series for the NARVAL, SOPHIE, and UVES data, respectively. Arrows underneath indicate the observational phases.

surface shear parameter. The best fit yields solar-type equatorial acceleration:

$$\Omega(\beta) = 20.763\ (1 - 0.053 \sin^2 \beta)\ [^\circ/\mathrm{d}]. \quad (2)$$

## 5. Discussions and conclusion

The outcome of our new cross-correlation study seems to be fairly consistent with the result in Paper I, where $\alpha$ of $0.049 \pm 0.003$ was derived. To test the reliability of our method and result we repeated the correlation study, but instead of using the combined Doppler images in Fig. 1, we started from individual reconstructions, i.e., we used Doppler images that are recovered individually for a single mapping line. This way we have four maps (Fe I-6411, Fe I-6421, Fe I-6430, and Ca I-6439) for each dataset separately, thus 12 cross-correlations could be achieved and finally averaged. We expect that this way the S/N of the DR pattern in the ultimate averaged CCF map will improve.

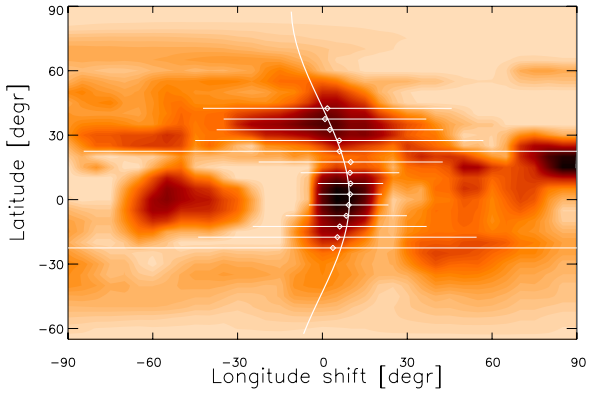


**Fig. 2.** Applying the ACCORD technique for the three available Doppler images plotted in Fig. 1. The better correlation on the resulting CCF map is represented by darker shade. The average longitudinal cross-correlation functions in bins of 5° are fitted by Gaussian curves (Gaussian peaks are indicated by dots, the FWHMs by horizontal lines). The continuous line represents the best-fit quadratic DR law.

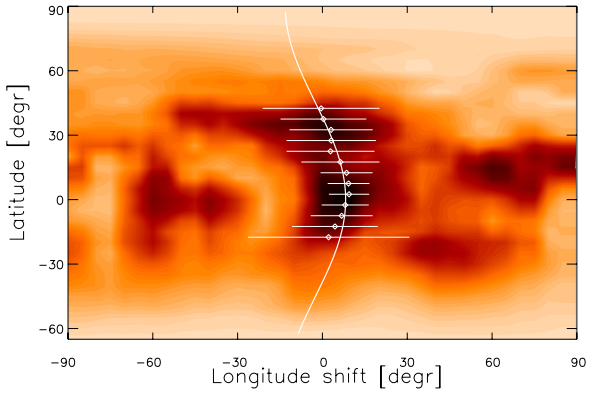


**Fig. 3.** Applying the ACCORD technique for the individual Doppler reconstructions using Fe I-6411, Fe I-6421, Fe I-6430 and Ca I-6439 mapping lines separately. Otherwise as in Fig. 2.

The result with the fitted DR pattern is shown in Fig. 3 and yields nearly the same DR law as Eq. (2):

$$\Omega(\beta) = 20.689\,(1 - 0.055\sin^2\beta)\ [^\circ/\mathrm{d}], \qquad (3)$$

but the relative height of the fitted "ridge" in the CCF landscape (i.e., the maxima of the Gaussian peaks) has significantly (≈40% on average) risen, compared to the one in Fig. 2. We can also estimate the errors of the derived parameters given in Eq. (3) by carrying out the whole process, but with using only three mapping lines from the available four, i.e., we performed four cross-correlation studies separately and estimated the error bars from the 1-$\sigma$ of the obtained DR parameters, obtaining $\varepsilon(\Omega_{\rm eq}) = \pm 0.056\,^\circ$/d and $\varepsilon(\alpha) = \pm 0.0022$. We consider this result as a proof of the reliability and robustness of the ACCORD technique. A comparative summary of the derived DR parameters is given in Table 2.

Theoretical calculations predict that across the H-R diagram DR becomes stronger with increasing rotation period and evolutionary status (Kitchatinov & Rüdiger 1999). Still, $\zeta$ And shows relatively weak surface differential rotation. This may be explained by large starspots that do not follow the stellar surface flows because they are anchored at different depths in the convection zone. Recent investigations by Korhonen & Elstner (2011) using dynamo models showed that the DR that is much weaker than what is used in the model is recovered when only the large-scale dynamo field is considered. The real input DR law can only be recovered when the model also includes small-scale fields. The question is whether or not large starspots can really be caused by small-scale magnetic fields.

**Table 2.** Comparing the DR parameters.

| $\Omega_{\rm eq}$ [°/d] | $\alpha$ | LT[a] [d] | Note |
|---|---|---|---|
| 19.027 | 0.049 | 381 | from Paper I |
| 20.763 | 0.053 | 332 | using combined images |
| 20.689 | 0.055 | 315 | using separate reconstructions |

**Notes.** [(a)] Time needed by the equator to lap the pole by one full period.

According to Kitchatinov & Rüdiger (2004), giant stars in close binary system, e.g., RS CVn-type binaries, can also show anti-solar differential rotation, where the equator rotates slower than the poles. This type of a DR law has been detected, for example, in $\sigma$ Gem (Kővári et al. 2007a). Kitchatinov & Rüdiger (2004) attributed the anti-solar differential rotation to a strong meridional flow, which could be caused by barocline driving due to large thermal spots or by field-forcing of a close companion. In accordance with this, a poleward meridional flow has been reported for $\sigma$ Gem with an average velocity of 350 km s$^{-1}$ (Kővári et al. 2007a). On the other hand, no sign of this meridional flow is seen on $\zeta$ And (Paper I). This observed difference between $\zeta$ And and $\sigma$ Gem can be rooted in the different system geometry and dynamics (Kővári et al. 2012). Distortion and tidal forces could account for the converse DR in these two cool giants.

*Acknowledgements.* Zs.K., L.K., and K.V. are grateful to the Hungarian Science Research Program (OTKA) for support under the grant K-81421. This work is supported by the "Lendület" Young Researchers' Program of the Hungarian Academy of Sciences. H.K. acknowledges the support from the EC under the Marie Curie IEF Programme in FP7.

## References

Aurière, M. 2003, in ESA Publ. Ser. 9, ed. J. Arnaud, & N. Meunier, 105
Barnes, J. R., Collier Cameron, A., Lister, T. A., et al. 2005, MNRAS, 356, 1501
Campbell, W. W., Moore, J. H., Wright, W. H., & Duncan, J. C. 1911, Lick Observatory Bulletin, 6, 140
Dekker, H., D'Odorico, S., Kaufer, A., et al. 2000, SPIE, 4008, 534
Donati, J.-F., & Collier Cameron, A. 1997, MNRAS, 291, 1
Eaton, J. A. 1995, AJ, 109, 1797
Gilliland, R. L., & Dupree, A. K. 1996, ApJ, 463, L29
Hussain, G. A. J., Allende Prieto, C., Saar, S. H., & Still, M. 2006, MNRAS, 367, 1699
Joy, A. H., & Wilson, R. E. 1949, ApJ, 109, 231
Kitchatinov, L. L., & Rüdiger G. 1999, A&A 344, 911
Kitchatinov, L. L., & Rüdiger G. 2004, AN, 325, 496
Korhonen, H., & Elstner, D. 2011, A&A, 532, A106
Korhonen, H., Wittkowski, M., Kővári, Zs., et al. 2010, A&A, 515, A14 (Paper II)
Kővári, Zs., Strassmeier, K. G., Granzer, T., et al. 2004, A&A, 417, 1047
Kővári, Zs., Bartus, J., Strassmeier, K. G., et al. 2007a, A&A, 474, 165
Kővári, Zs., Bartus, J., Strassmeier, K. G., et al. 2007b, A&A, 463, 1071 (Paper I)
Kővári, Zs., Bartus, J., Kriskovics, L., et al. 2012, in From Interacting Binaries to Exoplanets: Essential Modeling Tools, ed. M. Richards, & I. Hubeny (Cambridge: Cambridge Univ. Press), IAU Symp., 282, in press
Monnier, J. D., Zhao, M., Pedretti, E., et al. 2007, Science, 317, 342
Perruchot, S., Kohler, D., Bouchy, F., et al. 2008, Proc. SPIE, 7014, 70140J
Piskunov, N. E., Tuominen, I., & Vilhu, O. 1990, A&A, 230, 363
Reimers, D. 1980, in 2nd European IUE Conf., ed. B. Battrick, & J. Mort, ESA SP, 157, 77
Rice, J. B., Wehlau, W. H., & Khokhlova, V. L. 1989, A&A, 208, 179
Schrijver, C. J., Mewe, R., & Walter, F. M. 1984, A&A, 138, 258
Strassmeier, K. G., Hall, D. S., Boyd, L. J., & Genet, R. 1989, ApJS, 69, 141
Vogt, S. S., Penrod, G. D., & Hatzes, A. P. 1987, ApJ, 321, 496
Weber, M. 2007, AN, 328, 1075
Weber, M., & Strassmeier, K. G. 2001, A&A, 373, 974